

Chapter 3

CWDM routing for access networks

This chapter introduces the concept of coarse and dense WDM grid integration and its adaptation in access networks to map for the first time selective closely-spaced wavelengths into coarse passband windows of an AWG, exhibiting coarse-fine grooming. To that extent, flat and Gaussian coarse AWG passband profiles are simulated in virtual photonics Inc. (VPI) modelling, to evaluate individual grooming capabilities by means of their broad bandwidth, insertion loss, adjacent channel crosstalk and very importantly, polarisation dependency.

3.1 Principle of coarse-fine grooming operation

Having established deployment and operational costs in association with providing increased network and service penetration crucial for the application and evolution of access network technologies, the cost-effectiveness and scalability of CWDM, to supply a clear growth path by means of DWDM, constitute powerful characteristics in enhancing TDM operation assuming that the network traffic will not exceed the capacity of 18 wavelengths defined by ITU-T [1] in the near future [2-4]. Although extensive proposals of hybrid TDM/DWDM architectures have been investigated [5, 6], as presented in chapter 2, CWDM has not been collectively examined with its potential to enhance standard access networks. Consequently, according to the best-of-both-worlds approach [7, 8], to map dense wavelengths into broad channels of add/drop multiplexers located in RNs of a ring topology metro network, Figure 3-1 demonstrates how that approach would work.

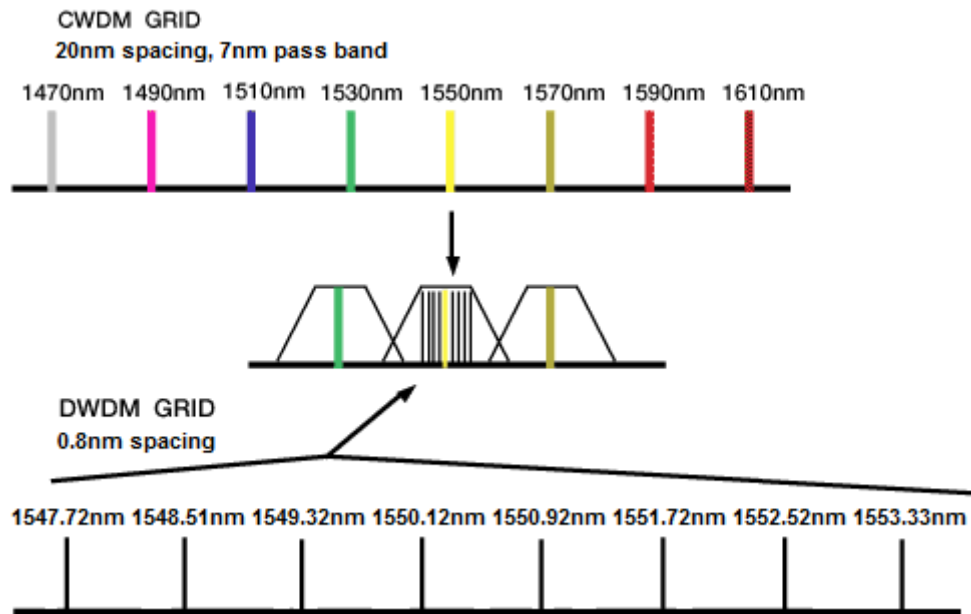


Figure 3-1 Best-of-both-worlds - DWDM grid fits into the CWDM grid [7]

The top spectrum in the figure displays 8 CWDM-grid wavelengths [1] ranging from 1470 nm to 1610 nm, while the bottom spectrum represents part of the DWDM-grid C band [9], including a set of 8, 0.8 nm-spaced, wavelengths. Subsequently, the middle spectrum illustrates how a CWDM filter of an add/drop multiplexer, creates a broad window over each of the individual CWDM-grid wavelengths, consequently allowing for the set of 8 dense wavelengths to be mapped into the CWDM wavelength grid.

The property of this coarse and dense multiplexing technique could be used in access networks to display parallel routing of TDM and WDM-PONs in a single platform to guarantee smooth upgradability, scalability, transparency and cost-effectiveness [10-13]. In that direction, an innovative access routing scheme is proposed, employing the coarse passbands of an $N \times N$ AWG, each of which creates a 7 nm-wide passband window, mapped over a set of dense wavelengths to exhibit coarse-fine grooming in the access network.

3.2 Array waveguide grating features for coarse-fine grooming

Commercial interest in AWG devices has been rapidly increasing by means of enhancing capacity and flexibility in access networks [14]. A variety of AWG properties, such as their reciprocal nature [15], free spectral range (FSR) periodicity, low insertion loss, diverse passband profiles and Latin-routing capabilities [15], depending on design, have been utilised to demonstrate diverse access networks [5, 6, 16, 17], employing in their majority dense AWG devices to achieve greater scalability and extended penetration. To realise coarse-fine grooming in the access network, allowing concurrent routing of different multiplexing PON technologies in a single infrastructure, coarse AWG prototypes have been presented [18-22], although still to become commercial available, comprising in their majority four 7 nm-wide channels with spacing of 20 nm corresponding to the ITU-T coarse wavelength grid [1].

Figure 3-2(a) shows the block diagram of a typical 4×4 coarse AWG utilising four channels λ_{1-4} . Each of the four input ports of the device can carry any of the four coarse channels. The channels carried by input port 1 are distributed to output ports 1-4 in such way that output port 1 carries λ_1 and output port 4 carries λ_4 . The four channels carried by input port 2 are distributed in the same form, however cyclically rotated by 1 in such way that channels λ_{1-4} are routed to output ports 4 to 3 respectively. In this way, channels can be routed from any of the four input

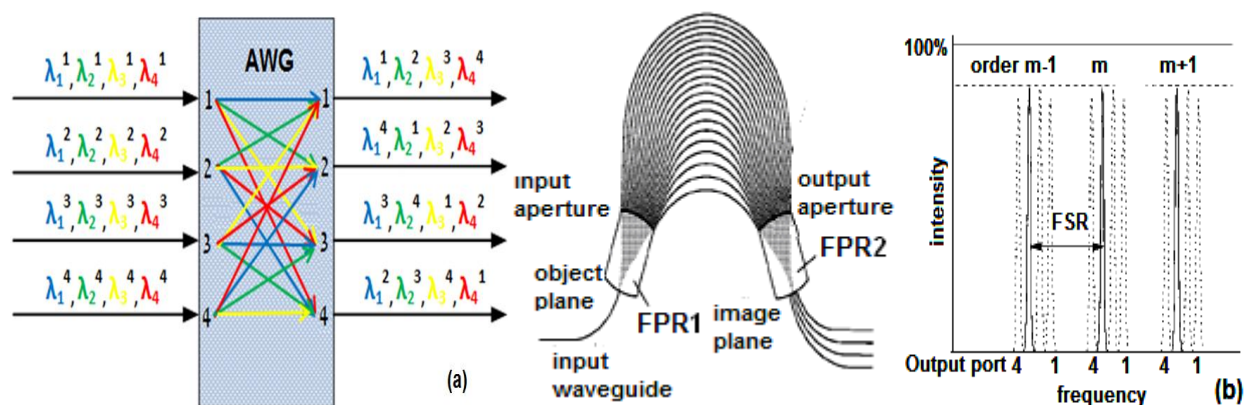


Figure 3-2 (a) Block diagram of a 4×4 coarse AWG (b) Functional diagram of an AWG [14]

to any of the four output ports and vice-versa using the Latin-routing property of the AWG [15]. In order to achieve this interconnection pattern, the number of operating channels and the channel spacing of the AWG must be chosen such that the channel spacing times the number of input/output (I/O) ports is equal to the FSR of the device.

Figure 3-2(b) shows the functional diagram of a $1 \times N$ AWG, utilised to describe the basic operation of an $N \times N$ AWG. Light couples from the input waveguide into free propagation region (FPR1) and as a result scatters into the arrayed waveguides. The length of each waveguide increases linearly compared to its previous. In case the central channel is utilised, light will focus at the midpoint of the image plane at the end of FPR2, subsequently terminated to an output waveguide, representing an output port of the AWG. Different channels at the AWG input will introduce different phase changes along the output plane of the array waveguide, allowing the focal point to be relocated at the end of the FPR2 and subsequently to be picked up by different output port. It has been previously reported that the response of the phased array is shown to be periodical, as shown also in Figure 3-2(b) [14]. In the Figure, two channels separated by an FSR, representing a period in the frequency domain, applied at the same input port of the AWG, will focus and leave via the same output waveguide independently of their wavelength since their phase at the outputs is the same.

With particular emphasis in exhibiting coarse-fine grooming, the 7 nm-wide AWG passband profile, whether of Gaussian or flat-top response, and corresponding insertion loss, crosstalk isolation and the most critical polarisation dependency figures become decisive factors in network design since they could restrict multi-wavelength operation within the coarse passbands at ever increasing subscriber volume and aggregate data rates.

3.2.1 Insertion loss

Typical loss figures reported for prototype coarse AWGs are in the range of 5 dB [23] to 8 dB [22]. These loss figures are expected to be increased by up to 3 dB using a Gaussian channel AWG as opposed to its flat counterpart, potentially affecting the multi-wavelength transmission within the passband. This is particularly true in the case for ONUs of a WDM-PON corresponding to wavelengths positioned closer to either edges of the passband, and as a result experience greater loss.

3.2.2 Crosstalk

Crosstalk in practical devices is originated from imperfections in the fabrication process [14] resulting in phase errors [23]. Typical crosstalk isolation figures reported for coarse AWGs are in the range of 20 dB [23] to 16 dB [20], potentially to be enhanced as a matter of improving the fabrication process and technology. Consequently, the crosstalk has the potential to impose interference between adjacent coarse passbands of the AWG and as a result to degrade the transmission performance of individual wavelengths representing ONUs within the passband.

3.2.3 Polarisation dependency

The AWG may be polarisation-sensitive if its waveguides are polarisation-dependent, i.e. the propagation constants of the fundamental transverse electric (TE) and transverse magnetic (TM) waveguide modes are different [14]. This induces polarisation-dependent wavelength (PDW) shift [23], for which the TM spectral response is shifted with respect to the TE response, consequently resulting in polarisation-dependent loss (PDL) [24] and polarisation mode dispersion (PMD). Based on wide passband AWG channels, the PDW shift should not be a major obstacle in CWDM applications due to insignificant PDL in the middle of each passband, where the operating wavelength is positioned and is usually employed to serve a TDM-PON. However, it is expected to restrict multi-wavelength operation within the passband [24],

particularly affecting those ONUs of a WDM-PON represented by wavelengths positioned at either edges of the passband where positive or negative shifting induces extended PDL. Flattening the passband of a device through design modifications could minimise the PDL associated with this shift [25], allowing the specifications for multi-wavelength DWDM applications to be met with those of CWDM applications.

3.3 Coarse AWG simulation model

Both the flat and Gaussian AWGs have been modelled and investigated since it was previously shown that their corresponding passband profiles have a direct impact on the various AWG transmission characteristics such as channel loss and PDL, depending on the location of the wavelength within the passband. To begin with, a 4×4 flat channel AWG has been modelled to comply with the commonly agreed channels count of N×N products.

3.3.1 Flat channel response

Table 3-1 describes the routing properties of a 4×4 flat channel AWG, employing 4 coarse channels centred at λ_1 , λ_2 , λ_3 and λ_4 , corresponding to 1530 nm, 1550 nm as central channel, 1570 nm and 1590 nm, collectively occupying an FSR of 80 nm. The input and output ports in the table represent either downstream or upstream transmission directions due to the AWG's reciprocal nature. According to the table, channels λ_{1-4} carried by input port 2 are routed from output ports 4 to 1 respectively. Subsequently, the four channels carried by input port 3 are distributed in the same form, however cyclically rotated by 1 in such way that channels λ_1 , λ_2 , λ_3 and λ_4 are routed to output ports 3, 2, 1 and 4 respectively. Accordingly, the same form of routing is applied to all other input ports in that order.

Table 3-1 Flat response coarse 4×4 AWG routing table

Input port	Output port			
	1	2	3	4
1	λ_1	λ_4	λ_3	λ_2
2	λ_4	λ_3	λ_2	λ_1
3	λ_3	λ_2	λ_1	λ_4
4	λ_2	λ_1	λ_4	λ_3

The transmission spectrum of the coarse AWG as produced in VPI is displayed in Figure 3-3. In order to produce the figure, the AWG input port 2 was scanned with wavelengths in the range of 1510 nm to 1610 nm and the power levels of all 4 output ports were recorded

simultaneously with an optical spectrum analyser. Subsequently, the transmission spectra exhibit adjacent channels crosstalk isolation greater than 20 dB and channel insertion loss of 5 dB. More specific modelling details will be explored in the following section of the chapter.

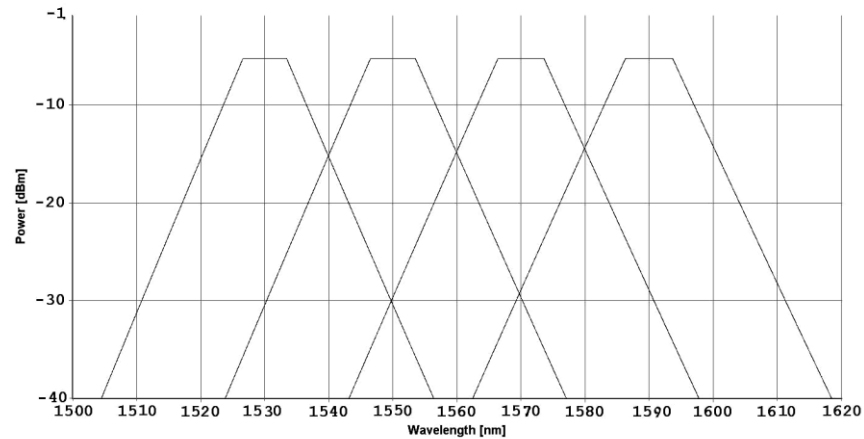


Figure 3-3 Flat response AWG transmission spectra

To get deeper into each coarse passband's characteristics, critical for the device routing performance when incorporated into the network, Figure 3-4 displays the AWG central channel at $\lambda_2=1550$ nm, exhibiting 7 nm flat-top spectral width at 0 dB and 12 nm-wide at 3 dB. The central channel response comprises only the TE response at this stage for the purpose of demonstrating the AWG preliminary routing capabilities, although the TM response is also necessary to be modelled since it induces significant PDL that affects wavelengths transmission over the passband, and as a result will be investigated in the following chapter.

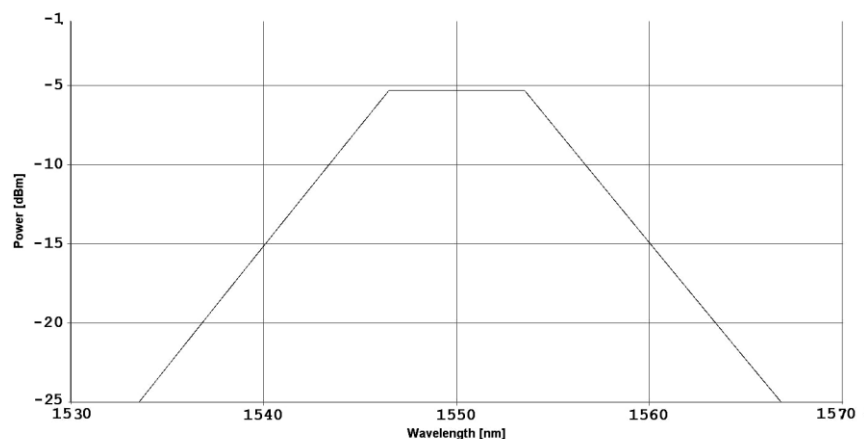


Figure 3-4 Flat response AWG central channel spectra

To demonstrate simultaneous transmission of standard 50 GHz, ITU-T grid wavelengths over the previously defined AWG coarse passbands and their routing on the basis of distinctive coarse channels rather than individual wavelengths, Figure 3-5 displays the channel response at $\lambda_2=1550$ nm encompassing 16, 0.4 nm-spaced wavelengths ranging from $\lambda_2^1=1553.33$ nm to $\lambda_2^{16}=1547.32$ nm, to represent 16 ONUs of a physical PON collectively transmitted over a network. Since the channel spectrum displays a 7 nm-wide passband window at 0 dB output power variation, over which the wavelengths are mapped, they are all routed over the passband to the same AWG output, in the sense of a single CWDM channel without any power variations. Similar results were also recorded for all four passbands. Likewise, as it will be further discussed in chapter 8, this routing approach has a potential to be achieved using a wavelength switch, capable to cross-connect wavelengths between any I/O ports, however as opposed to the AWG employing reciprocal infrastructure, it offers only unidirectional flow due to its active nature.

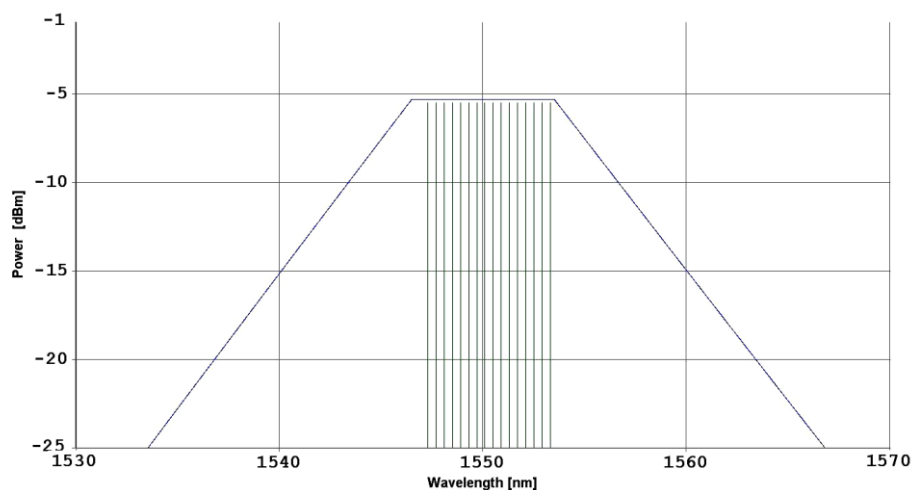


Figure 3-5 Flat coarse passband in multi-wavelength operation

3.3.2 Gaussian channel response

As opposed to the flat channel AWG, the Gaussian device was previously shown to utilise additional 3 dB insertion loss and extended PDL, particularly at the passband edges, on top of the device insertion loss. Consequently, a study was conducted with the aim to implement a Gaussian device that demonstrates typical parameter values common among all proposed prototypes [18-20, 22, 23], such as wavelength operation range, passband bandwidth, channel spacing, insertion loss and channel uniformity, and specialised parameters unique to the polarisation sensitivity and crosstalk isolation. In that sense, a 5×5 AWG prototype [23] which has been extensively developed [26, 27] and has demonstrated improved specialised parameters performance was selected for modelling. This prototype device comprises 5×5 I/O ports [23], employing five coarse channels at $\lambda_0, \lambda_1, \lambda_2, \lambda_3$ and λ_4 , over an FSR of 130 nm, corresponding to channels at 1510 nm, 1530 nm, 1550 nm, 1570 nm and 1590 nm. Table 3-2 shows the routing properties of the AWG, for which the shaded areas in the table represent wavelengths out of use. According to the table, channels λ_{0-4} carried by input port 3 are routed from output ports 5 to 1 respectively. Subsequently, the five channels carried by input port 4 are distributed and cyclically routed in the same way to the flat AWG.

Table 3-2 Gaussian response coarse 5×5 AWG routing table

Input port	Output port				
	1	2	3	4	5
1			λ_4	λ_3	λ_2
2		λ_4	λ_3	λ_2	λ_1
3	λ_4	λ_3	λ_2	λ_1	λ_0
4	λ_3	λ_2	λ_1	λ_0	
5	λ_2	λ_1	λ_0		

The transmission spectra of the simulation results for the 5×5 coarse channel AWG is displayed in Figure 3-6, exhibiting adjacent channels crosstalk isolation greater than 34 dB, which is limited due to phase-errors in the fabrication process [23], and insertion loss of 5 dB at the

central channel with no more than 1 dB loss uniformity across the entire FSR. The crosstalk isolation figure is particularly important for multi-wavelength operation when transmitting at either edges of the passband where the crosstalk isolation is reduced by approximately 3 dB due to the Gaussian response.

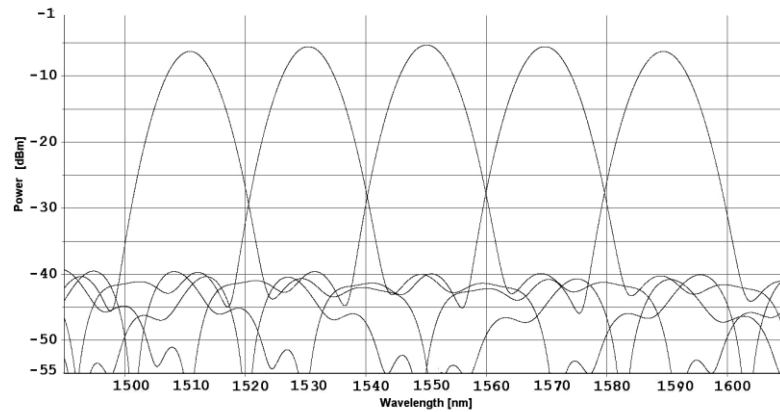


Figure 3-6 Gaussian response AWG transmission spectra

Figure 3-7 displays the device TE response central channel at $\lambda_2=1550$ nm exhibiting 7 nm spectral width at 3 dB, as opposed to the flat response which exhibited similar spectral width at 0 dB. This allows for power variation of up to 3 dB, in addition to the 5 dB insertion loss, among the 16 ONUs of a physical PON mapped within the passband.

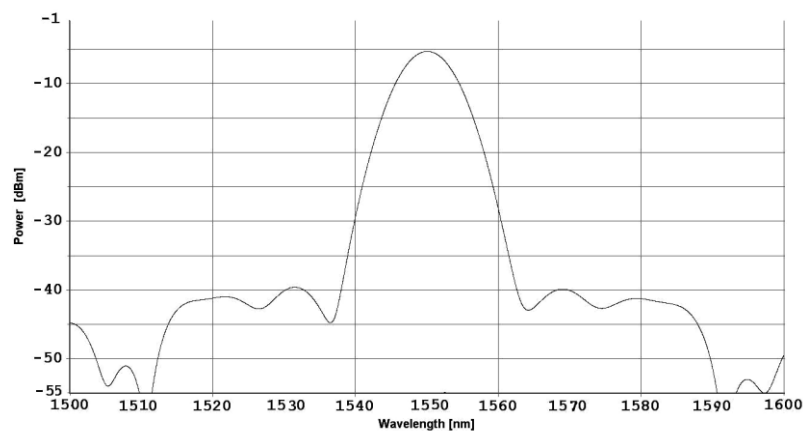


Figure 3-7 Gaussian AWG central channel spectra

In relation to the AWG's routing capability, Figure 3-8 displays the Gaussian channel at $\lambda_2=1550$ nm with the same 16, 0.4 nm-spaced wavelengths employed in the flat model multiplexed across the passband. Although all 16 wavelengths are still mapped over the AWG passband successfully and as will be shown in following sections routed jointly by way of the 1550 nm coarse channel through to the same network destination, the displayed 7 nm-wide channel Gaussian response at 3 dB imposes an overall power variation of 3 dB between the central wavelength at $\lambda_2^1=1550.12$ nm and $\lambda_2^{16}=1547.32$ nm right at the passband edges. Having established the 3 dB additional loss for the latter, further investigation needs to take place to demonstrate the performance of the higher attenuated wavelengths in the channel since they will be representing ONUs of the same physical PON and their consistent performance is critical for the network operation.

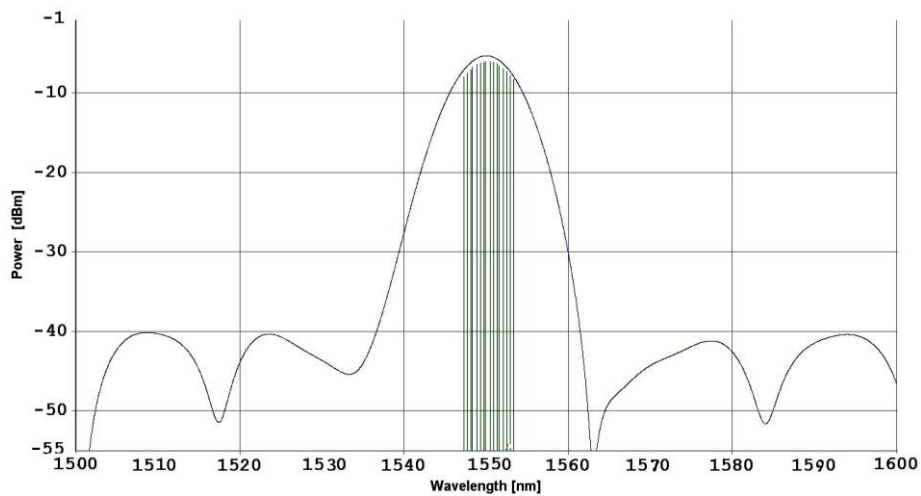


Figure 3-8 Gaussian passband in multi-wavelength operation

3.4 Coarse AWG router modelling

In order to establish the viability of the proposed routing scheme, physical-layer models for both the Gaussian and flat-top AWG devices were devised in VPI simulation platform. Particular attention was given to the polarisation dependency in both models since it has been established as a critical parameter due to the extended AWG passband widths as opposed to dense devices [28] by allowing for PDW shift to be demonstrated, controlled by the AWG physical parameters not accounted-for in standard VPI modules.

3.4.1 Flat response

Since flat AWGs are non-standard VPI modules, the 4×4 flat-top model displayed in Figure 3-9, was designed using a combination of customised 1×4 demultiplexers, and standard signal combiners, where each demultiplexers is realised using a set of standard flat-top optical filters representing the device passband windows. Each of the four input ports on the left hand side of the AWG is initially applied at a 1×4 demultiplexer utilised to route the input wavelength to one of 4 possible outputs depending on the wavelength used. Subsequently, each of demultiplexer outputs is interconnected to the designated output ports of the AWG via the 4 signal combiners. This interconnection pattern corresponds to the routing properties shown initially in Table 3-1.

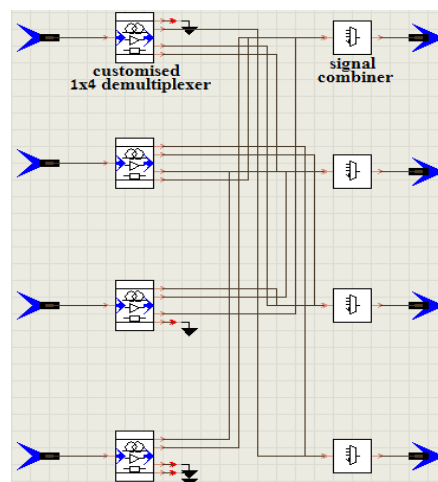


Figure 3-9 Flat response AWG modelling based on customised 1×4 demultiplexers

Figure 3-10 displays the modelling of the 1×4 demultiplexer. Initially, an optical attenuator is used to model the insertion loss of each AWG channel. The attenuator output is directly connected to four polarisation beam splitters (PBSs) where their x and y coordinated outputs are applied at the TE and TM mode optical filters respectively to demonstrate PDW shifting. The outputs of each pair of filters, corresponding to a single coarse channel, are combined using a polarisation beam combiner (PBC) and subsequently applied at the output port of the demultiplexer. To control the PDW shift figure, the central wavelength (referred as frequency in the simulation tool) used by each of the TM mode filters, representing the TM passband windows of the AWG, is shifted by a selected amount in nm units.

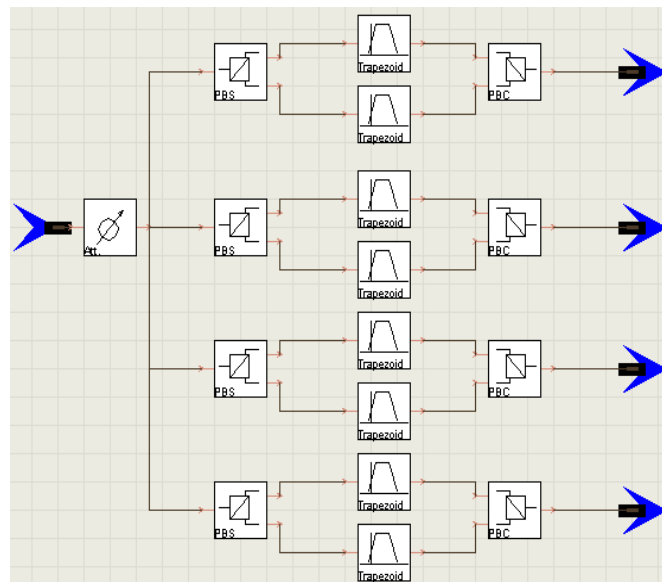


Figure 3-10 Flat response AWG - 1×4 demultiplexer modelling based on optical filters

VPI Table 3-3 includes the design parameters of the TE optical filter, representing the central channel at 1550 nm. The zero dB bandwidth parameter is set to 875 GHz to demonstrate 7 nm-wide flat response at 0 dB. In addition, the cut-off bandwidth parameter is set to 4.2 THz to allow 12 nm-wide at 3 dB channel response, and the cut-off magnitude parameter is set by the variable Xtalk to achieve 20 dB adjacent channel crosstalk isolation.

Table 3-3 TE flat-top optical filter design parameters

→	f	CenterFrequency	2.9979e8/1550e-9	Hz
→	f	Zero_dB_Bandw	875e9	Hz
→	f	CutoffMagnitude	Xtalk	dB
→	f	CutoffBandwidth	4.2e12	Hz

Likewise, VPI Table 3-4 includes the design parameters for the TM mode optical filter. To account for polarisation dependency, the filter central wavelength encompasses shifting capabilities expressed by the parameter nm_shift in nm units. All other parameters are identical to their TE mode filter counterparts.

Table 3-4 TM flat-top optical filter design parameters

→	f	CenterFrequency	2.9979e8/(1550e-9 - nm_shift*1e-9)	Hz
→	f	Zero_dB_Bandw	875e9	Hz
→	f	CutoffMagnitude	Xtalk	dB
→	f	CutoffBandwidth	4.2e12	Hz

3.4.2 Gaussian response

The 5×5 Gaussian coarse AWG [23], displayed in Figure 3-11, comprises two identical standard Gaussian AWG modules, as opposed the use of filters for the flat AWG, employed to accommodate the two waveguide transmitted modes TE and TM. As displayed in the figure, each of the five input ports of the model is applied at a PBS, where its x and y coordinated outputs are applied at the corresponding TE and TM mode AWGs. Subsequently, the outputs of the two AWGs are combined using PBCs and applied at each of the corresponding output ports of the model. To shift the TM passband with respect to its TE counterpart, the central wavelength in the TM mode AWG can be offset by a selected amount in nm units. Also, as opposed for the flat AWG, the Gaussian prototype device waveguide physical parameters [23] and phase-error figure [29] were incorporated into both AWG modules providing realistic performance of the model.

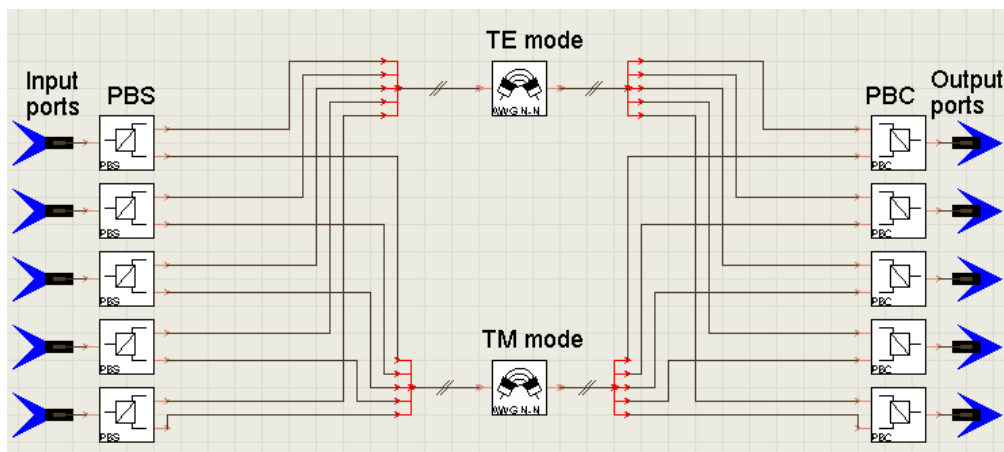


Figure 3-11 5×5 Gaussian response AWG modelling

VPI Table 3-5 includes the design parameters for the TE mode AWG. The central wavelength is set to 1550.1 nm [23] with 5 dB loss [23]. In addition, an FSR of 16.25 THz and channel spacing of 2.45 THz are utilised corresponding to 130 nm and 20 nm of the prototype AWG [23]. Also, its waveguides physical parameters [23] such as their dimensions and separation figures are applied directly into the AWG module. Finally, a random-phase-noise parameter corresponding to phase-errors that have the potential to limit the adjacent crosstalk isolation can be selected for the model using the variable Phase_Error in degrees units.

Table 3-5 TE Gaussian passband design parameters

→	f	CenterFrequency	2.9979e8/(1550.1e-9)	Hz
→	f	LossAtCenterFrequency	5.0	dB
→	f	FreeSpectralRange	16.25e12	Hz
→	f	ChannelSpacing	2.45e12	Hz
→	i	NumberOfChannels	5	
→	f	WaveguideWidth	4.0e-6	m
→	f	SlabModeIndex	1.478	
→	f	NormalizedPropConst	0.6	
→	f	InputOutputWaveguidesSep	10e-6	m
→	f	ArrayedWaveguidesSep	4e-6	m
→	f	RandomPhaseNoise	Phase_Error	deg

VPI Table 3-6 includes the design parameters for the TM mode AWG. Although all other physical parameters are identical to their TE mode AWG counterparts, the central wavelength of the model facilitates shifting features articulated by the parameter nm_shift in nm units to demonstrate shifting of the TM response.

Table 3-6 TM Gaussian passband design parameters

→	f	CenterFrequency	2.9979e8/(1550.1e-9 - nm_shift*1e-9)	Hz
→	f	LossAtCenterFrequency	5.0	dB
→	f	FreeSpectralRange	16.25e12	Hz
→	f	ChannelSpacing	2.45e12	Hz
→	i	NumberOfChannels	5	
→	f	WaveguideWidth	4.0e-6	m
→	f	SlabModeIndex	1.478	
→	f	NormalizedPropConst	0.6	
→	f	InputOutputWaveguidesSep	10e-6	m
→	f	ArrayedWaveguidesSep	4e-6	m
→	f	RandomPhaseNoise	Phase_Error	deg

The modelling of the Gaussian AWG to the stringent specifications of the 5×5 Gaussian AWG prototype [23] offers, except for the most practical specifications to implement commercialised coarse AWGs in the future, the most effective means of evaluating the performance of the modelled device in contrast to the recorded prototype figures [23]. To that extent, individual transmission spectra are shown in Figure 3-12, confirming comparable AWG passband characteristics, with measured insertion loss of 5 dB at the central channel and no more than 1 dB loss variations across the entire FSR. In addition, as expected, each AWG channel spectrum exhibits 7 nm spectral width at 3 dB.

Nevertheless, as shown in Figure 3-12(b), the modelled AWG exhibits crosstalk isolation of 35 dB compared to 20 dB of the prototype device in Figure 3-12(a). This discrepancy could be justified if it is taken into account that preliminary simulation-based results of the prototype device produced crosstalk isolation of 65 dB [30] that was later significantly reduced in the fabrication process due to unrecorded phase-errors between the array waveguides [30]. To that extent, worst case 270° phase-errors were included in the VPI model as suggested by a major photonic devices vendor [29]. Although the experimental 20 dB crosstalk isolation of the prototype device was not achieved, the produced figure of 35 dB adds confidence since it was reproduced under realistic conditions.

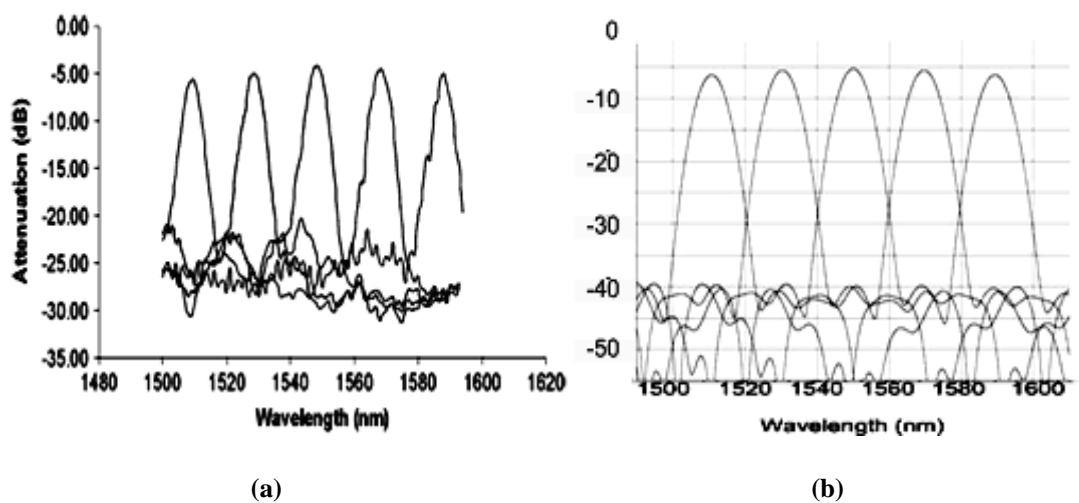


Figure 3-12 AWG transmission spectra comparison (a) prototype [23], modelling (b)

3.5 Summary

This chapter introduced initially the best-of-both-worlds approach [7] and its merits in accumulating wavelength count, followed by suggestions in developing broadband access networks with particular emphasis in the integration of various multiplexing formats over PONs to exhibit access network transparency, smooth upgradability, scalability and cost-effectiveness [10-13].

Subsequently, the attractive features [17] of coarse AWGs as a routing device were analysed to demonstrate coarse-fine grooming by means of employing each coarse passband channel of an $N \times N$ AWG to collectively route wavelengths to ONUs of individual physical PON locations in a multiple PON access network architecture terminated to a single OLT [20]. To that extent Gaussian and flat-top coarse AWG devices were modelled and evaluated, employing multiple 7 nm-wide passband windows to allow up to 16, 50 GHz ITU-T wavelengths multiplexed over each of their passbands.

Preliminary grooming capabilities were demonstrated initially for a 4×4 flat-top response AWG, allowing all 16, 0.4 nm-spaced wavelengths ranging from 1553.33 nm to 1547.32 nm to be routed over the coarse channel at 1550 nm without any power variations. Modelling of the AWG was based on a combination of demultiplexers, taking into account polarisation dependency, passband width, insertion loss and adjacent channels crosstalk.

Since research in the area of coarse AWG prototypes has been focusing merely on Gaussian channel devices [18-20, 22, 23], a 5×5 Gaussian response AWG [23] was demonstrated, exhibiting channel spectral width of 7 nm at 3 dB. Consequently this allowed all wavelengths in the passband to be routed jointly with power variations of no more than 3 dB between the

central wavelength at 1550.12 nm and edge wavelengths at 1553.33 nm and 1547.32 nm. Modelling of the device was realised by employing two identical AWG VPI modules to accommodate the TE and TM passbands of a polarisation-dependent device [23], not supported in VPI modules.

For modelling evaluation purposes, the devised and prototype Gaussian AWGs were compared and contrasted. The simulated device exhibited comparable spectra characteristics to the prototype recorded figures, utilising similar channel spectral width and insertion loss of 5 dB with no more than 1 dB variations across the entire FSR. In addition, worst case 270° phase-errors were employed in the model, as advised by a major photonic devices vendor [29], to exhibit a worst case simulated crosstalk isolation of 35 dB.

3.6 References

- [1] ITU-T Recommendation: G.694.2, "Spectral Grids for WDM Applications: CWDM wavelength grid," 2003.
- [2] J. Wellen, R. Smets, W. Hellenthal, J. Lepley, I. Tsalamanis, S. Walker, A. Ng'oma, G.-J. R. Koonen, K. Habel, and K. D. Langer, "Towards High speed Access Technologies: results from MUSE," presented at SPIE Broadband Access Communication Technologies, Boston, MA, USA, 2006.
- [3] F.-T. An, D. Gutierrez, K. S. Kim, J. W. Lee, and L. G. Kazovsky, "SUCCESS-HPON: A Next-Generation Optical Access Architecture for Smooth Migration from TDM-PON to WDM-PON," *IEEE Communications Magazine*, vol. 43, pp. S40- S47, 2005.
- [4] K.-D. Langer, K. Habel, F. Raub, and M. Seimetz, "CWDM access network and prospects for introduction of full-duplex wavelength channels," presented at Conference on Networks & Optical Communications (NOC 2005), UCL, 2005.
- [5] C. Bock, J. Prat, and S. D. Walker, "Hybrid WDM/TDM PON using the AWG FSR and featuring centralized light generation and dynamic bandwidth allocation," *IEEE/OSA Journal of Lightwave Technology*, vol. 23, pp. 3981-3988, 2005.
- [6] D. J. Shin, D. K. Jung, H. S. Shin, J. W. Kwon, S. Hwang, Y. Oh, and C. Shim, "Hybrid WDM/TDM-PON With Wavelength-Selection-Free Transmitters," *IEEE/OSA Journal of Lightwave Technology*, vol. 23, pp. 187-195, 2005.
- [7] J. Aldridge, "The best of both worlds," *Lightwave Europe*, pp. 18-19, 2002.
- [8] R. Rastislav, "The utilization of the DWDW/CWDM combination in the metro/access networks," presented at Joint First Workshop on Mobile Future and Symposium on Trends in Communications (SympoTIC '03), Bratislava, Slovakia, 2003.

- [9] ITU-T Recommendation: G.694.1, "Spectral grids for WDM applications: DWDM frequency grid," 2002.
- [10] C.-H. Lee, S.-M. Lee, K.-M. Choi, J.-H. Moon, S.-G. Mun, K.-T. Jeong, J. H. Kim, and B. Kim, "WDM-PON experiences in Korea [Invited]," *OSA Journal of Optical Networking*, vol. 6, pp. 451-464, 2007.
- [11] T. Koonen, "Fiber to the Home/Fiber to the Premises: What, Where, and When?" *Proceedings of the IEEE*, vol. 94, pp. 911 - 934, 2006.
- [12] P. Chanclou, S. Gosselin, J. F. Palacios, V. L. Álvarez, and E. Zouganeli, "Overview of the Optical Broadband Access Evolution: A Joint Article by Operators in the IST Network of Excellence e-Photon/ONe," *IEEE Communications Magazine*, vol. 44, pp. 29-35, 2006.
- [13] F. Effenberger, D. Clearly, O. Haran, G. Kramer, R. D. Li, M. Oron, and T. Pfeiffer, "An introduction to PON technologies," *IEEE Communications Magazine*, vol. 45, pp. S17-S25, 2007.
- [14] M. K. Smit and C. v. Dam, "PHASAR-Based WDM-Devices Principles, Design and Applications (Invited)," *IEEE Journal On Selected Topics In Quantum Electronics*, vol. 2, pp. 236-250, 1996.
- [15] I. Tsalamanis, E. Rochat, and S. D. Walker, "Experimental demonstration of cascaded AWG access network featuring bi-directional transmission and polarization multiplexing," *OSA Optics Express*, vol. 12, pp. 764-769, 2004.
- [16] Y.-L. Hsueh, M. S. Rogge, W.-T. Shaw, L. G. Kazovsky, and S. Yamamoto, "SUCCESS-DWA: A Highly Scalable and Cost-Effective Optical Access Network," *IEEE Optical Communications*, vol. 42, pp. S24-S30, 2004.

- [17] M. C. Parker and S. D. Walker, "Splitters and arrayed-waveguide gratings for optical access: What's the difference? (Invited)," presented at Networks and Optical Communications (NOC 2006), Berlin, Germany, 2006.
- [18] H. C. Woei, N. A. Rahman, and S. Shaari, "Conventional Arrayed Waveguide Grating with 4 Channel Structure Design for CWDM," presented at International Conference on Semiconductor Electronics (ICSE), Kuala Lumpur, Malaysia, 2004.
- [19] T. Lang, J.-J. He, and S. He, "Cross-Order Arrayed Waveguide Grating Design for Triplexers in Fiber Access Networks," *IEEE Photonics Technology Lett.*, vol. 18, 2006.
- [20] N. Yurt, K. Rausch, A. R. Kost, and N. Peyghambarian, "Design and fabrication of a broadband polarization and temperature insensitive arrayed waveguide grating on InP," *Optics Express 'OSA'*, vol. 13, pp. 5535-5541, 2005.
- [21] S. Shaari and M. S. Kien, "Design implementation of up to 20 channel silica-based arrayed waveguide WDM," presented at International Conference on Semiconductor Electronics (ICSE), Kuala Lumpur, Malaysia, 2000.
- [22] J. L. Chemmanda, V. R. Pamidighantam, and S. Krishnamachari, "Design of Polymer Arrayed Waveguide Gratings for Access Networks and CWDM Applications," presented at Electronics Packaging Technology Conference (EPTC), 2003.
- [23] J. Jiang, C. L. Callender, C. Blanchetière, J. P. Noad, S. Chen, J. Ballato, and J. Dennis W. Smith, "Arrayed Waveguide Gratings Based on Perfluorocyclobutane Polymers for CWDM Applications," *IEEE Photonics Technology Letters*, vol. 18, pp. 370-372, 2006.
- [24] Y. Shachaf, C.-H. Chang, P. Kourtessis, and J. M. Senior, "Multi-PON access network using a coarse AWG for smooth migration from TDM to WDM PON," *OSA Optics Express*, vol. 15, pp. 7840-7844, 2007.

- [25] J. Jiang, C. L. Callender, C. Blanchetière, J. P. Noad, S. Chen, J. Ballato, and D. Smith, "Property-Tailorable PFCB-Containing Polymers for Wavelength Division Devices," *IEEE/OSA Journal of Lightwave Technology*, vol. 24, pp. 3227-3234, 2006.
- [26] J.-F. Viens, C. L. Callender, J. P. Noad, and L. Eldada, "Compact Wide-Band Polymer Wavelength-Division Multiplexers," *IEEE Photonics Technology Letters*, vol. 12, pp. 1010-1012, 2000.
- [27] L. Robitaille, C. L. Callender, and J. P. Noad, "Design and fabrication of low-loss polymer waveguide components for on-chip optical interconnection," *IEEE Photonics Technology Letters*, vol. 8, pp. 1647 - 1649, 1996.
- [28] ANDevices Inc., "NxN AWG multiplexers and demultiplexers Router Module," <http://www.andevices.com/PDF/APRTE.pdf>, 2007.
- [29] A. Wang, "Private communication." Fremont, CA: ANDevices, Inc, 2006.
- [30] J. Jiang, "Private communication." Ottawa, Canada: Communications Research Centre, 2006.